Volume 15 | Number 33 | 7 September 2019 | Pages 6607–6760

Soft Matter

rsc.li/soft-matter-journal

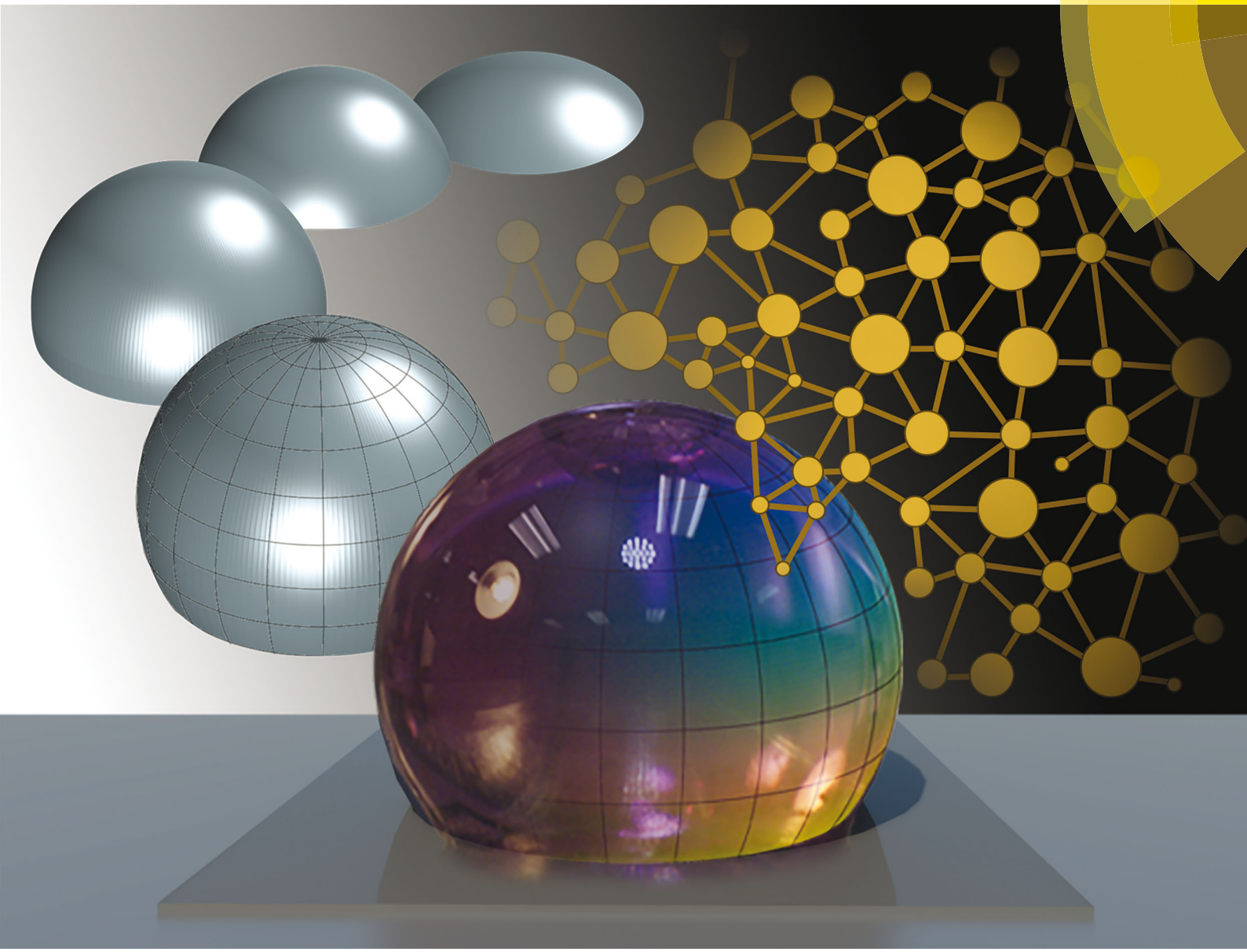

ISSN 1744-6848

ROYAL SOCIETY OF CHEMISTRY | Celebrating IYPT 2019

PAPER
Eduard Benet and Franck J. Vernerey
Dynamic competition of inflation and delamination in the finite deformation of thin membranes

Soft Matter

PAPER

View Article Online
View Journal | View Issue

Cite this: *Soft Matter*, 2019, **15**, 6630

Dynamic competition of inflation and delamination in the finite deformation of thin membranes

Eduard Benet and Franck J. Vernerey *

Received 23rd May 2019,
Accepted 12th July 2019

DOI: 10.1039/c9sm00988d

rsc.li/soft-matter-journal

The mechanics of blister delamination and growth plays a major role in a diversity of areas including medicine (skin pathology and mechanics of cell membranes), materials (adhesive and fracture) or soft robotics (actuation and morphing). The behavior of a blister in this context is typically difficult to grasp as it arises from the interplay of two highly nonlinear and time-dependent processes: membrane attachment and decohesion from a substrate. In the present work, we device a simplified approach, based on experimental systems, to predict the deformation path of a blister under various conditions. For this, we consider the problem of a growing blister made of a rubber-like membrane adhered on a rigid substrate, and develop a theoretical and experimental framework to study its stability and growth. We start by constructing a theoretical model of viscoelastic blister growth which we later validate with an experimental setup. We show that blister growth is controlled by the competition between two instabilities: one inherent to the rubber, and a second one pertaining to the adhesion with the substrate. Using these concepts, we show that a "targeted" stable blister shape can be achieved by controlling two parameters: the thickness of the film and the inflation rate.

1 Introduction

The study of blisters is often associated with pathologies of multilayered materials where one layer loses the cohesion that keeps it attached to its substrate. Indeed, blisters are a symptom of skin diseases such as burns,[1] and of poorly adhered industrial films such as paint[2] or paper.[3] Consequently, blistering and peeling tests are mostly used as methods for measuring the adhesion between two materials,[4,5] and have a high impact on the packaging of food and medical industries.[6,7] However, a variety of systems take advantage of the morphology changes that blisters provide and use them as an active mechanism. In nature, for instance, the finite deformation of membranes in the form of blisters is seen in the vocal sac of frogs[8] and in the skin papillae of some species of arthropods.[9] While it does not involve the delamination between two membranes, these skin morphing mechanisms are indeed based on the finite inflation of a constrained membrane. At a different scale, cellular blebbing is a process in which the outer lipid membrane of animal cells partially detaches from the inner cortex[10,11] and produces a blister that can be used as a motion mechanism.[12] The same concept has been studied and applied in the context of skin diseases,[13] where authors used a membrane inflation technique to induce the detachment and growth of new skin. Despite their disparity, controlling and harvesting these behaviors require a deep understanding of a common problem defined by the finite inflation and delamination of a thin, viscoelastic membrane. While the mechanics of blisters have been well-studied in the elastic case, the role of viscous effects influencing these processes is still poorly understood. Hence, the objective of this paper is to develop a theoretical framework to study the stability of blister growth and its impact on shape morphing technologies.

From a theoretical viewpoint, modeling the adhesion mechanics of viscoelastic blisters is a problem that requires the combination of three topics: the mechanics of membranes under finite strain, the mechanics of adhesion, and delamination dynamics. While only the second part is genuinely novel in a viscoelastic system, the problem cannot be explained without accounting for all three elements. First of all, understanding the adhesion stability of a membrane requires precise knowledge of its internal stresses as they are ultimately responsible for the pulling force that eventually breaks the adhesion.[14,15] However, while membrane theory is well-known in finite elasticity,[16,17] viscoelastic models are scarce in the literature. Furthermore, most common approaches, such as the Christensen model,[18–21] are phenomenological and thus provide little information on the molecular mechanisms driving these behaviors. To maintain a closer connection with the underlying physics,

Department of Mechanical Engineering, University of Colorado at Boulder, Boulder, Colorado, USA. E-mail: franck.vernerey@colorado.edu

this paper follows the recent approach of Benet *et al.* where the viscoelastic response of polymer membranes was modeled from the perspective of transient network theory (TNT).[22,23] Second, these stresses must be translated into quantifiable adhesion energy, which determines the conditions for delamination. In the case of stretchable membranes, the problem was initially approached from a small strain perspective. Authors such as Williams[24] developed analytical expressions to compute the energy released during membrane delamination. This approach was later extended to finite elasticity, where authors such as Nadler[25] and Long[26] stressed the importance of nonlinear terms. However, despite extensive follow-up work in understanding[27–30] and measuring[31–33] the different aspects of the adhesion of shells and membranes in finite strain, the role of viscosity in this process remains poorly understood. To the best of our knowledge, only the work of Srivastava[34] has discussed the viscous effects during the contact mechanics of a membrane, but a deep study on how they affect the energy release rate is still missing. Finally, this energy is used to construct a model that explains the spreading dynamics. In this paper, we build upon existing, well-accepted models[35] and implicitly incorporate the viscous effects through the previous two areas of study.

Overall, the main contribution of this paper relies on providing, for the first time, a combined model of a spreading viscous membrane which we use to study how the viscoelasticity affects the delamination of membranes. The results show that the growth of an elastic blister is a problem driven by competition between two known instabilities: one inherent to the rubber,[36] and a second one pertaining to the adhesion with the substrate.[37] Interestingly, the meeting of these two processes enables obtaining a variety of stable blister profiles by only adjusting the thickness of the film and the inflation rate. The paper is organized as follows. In Section 2, we discuss the mechanics of a viscoelastic, axisymmetric membrane. Section 3 derives an expression for the energy release rate, which is used in Section 4 to discuss the spreading of a blister. Finally, Section 5 shows an experimental validation and provides a discussion of the results.

2 Model

2.1 Equilibrium of a blister under finite deformation

To construct a viscoelastic model of a blister, we begin with a few notions in the theory of membranes used to derive its governing equations. A membrane is defined as a three-dimensional solid that has one dimension (its thickness h) significantly smaller than the others. This entails the following approximations: (a) stresses and strains are constant across the membrane thickness, (b) the stresses normal to the thickness can be neglected (plane stress assumption) and (c) bending moments are negligible compared to in-plane stresses. Mathematically, a membrane can therefore be described by its mid-plane surface, parameterized with two coordinates ξ^α ($\alpha = 1, 2$) immersed in a three-dimensional space. On this surface, internal forces are represented by a two-dimensional stress tensor $\boldsymbol{\sigma}$ whose components $\sigma^{\alpha\beta}$ represent the thickness average of the tangent Cauchy stress.[38] A similar thickness average of the balance of linear momentum then leads to the well-known governing equation of the mid-plane of a membrane[16] (see Appendix A for details):

$$\sigma^{\alpha\beta}|_\beta + f^\alpha = 0 \quad \sigma^{\alpha\beta}\kappa_{\alpha\beta} + f^n = 0 \tag{1}$$

where $\kappa_{\alpha\beta}$ is the curvature tensor and f^α and f^n correspond to the external pressures applied tangent and normal to the membrane, respectively. We here concentrate on the inflation of an axisymmetric blister (Fig. 1a) whose reference state is an unstretched circular membrane of radius R and thickness h_0. Under these axisymmetric conditions, the blister can first be parameterized by the arc length s of its cross-section and the revolution angle ϕ (details on Appendix B), such that only two components of the stress tensor are non-zero: the longitudinal stress σ^s and the hoop stress σ^ϕ (Fig. 1a). The position of the membrane at $\phi = 0$ can, therefore, be described by the radius $r(s)$ and the height $z(s)$ with respect to the center of the reference circle, and the governing eqn (1) simplifies to:

$$(\sigma^s)' + \frac{r'}{r}(\sigma^s - \sigma^\phi) + (r'^2 + z'^2)f^\alpha = 0 \tag{2a}$$

$$\sigma^s\kappa_1^1 + \sigma^\phi\kappa_2^2 + f^n = 0 \tag{2b}$$

where the apostrophes indicate a derivative with respect to s, and κ_β^α are the components of the mixed form of the curvature tensor (see details in Appendix A). For an axisymmetric surface, these curvatures relate to the mean curvature H by $H = \frac{1}{2}(k_1^1 + k_2^2)$. Thus, eqn (2b) can be understood by making an analogy to the Laplace law in fluid–fluid interfaces; *i.e.*, both equations use curvatures (k_1^1 and k_2^2) to relate internal pressure (f^n) and surface tension (σ^s and σ^ϕ). In other words, this relationship represents the equilibrium of normal (f^n) and tangential forces (f^α) acting along the membrane.

2.2 Viscoelastic constitutive relation

The viscoelastic constitutive relation of a polymer is then introduced by means of TNT,[22,39] an approach where the macroscopic response is derived based on the statistical description of the molecular chains and their degree of cross-linking. This theory conceptualizes a polymer as the superposition of N molecular networks, which are classified into two different types: permanent and dynamic (Fig. 1c). Permanent networks are characterized by permanent cross-links and thus display an elastic macroscopic response. By contrast, dynamic networks possess cross-links that constantly detach and reconnect at rates k_a and k_d, respectively. Macroscopically, such networks have the response of elastic fluids; *i.e.*, they respond elastically to fast loading, but relax and flow like a fluid at longer time scales. For the time, let us consider a single network, whose chain density is denoted by C. When the network is dynamic, only a fraction of these chains is fully connected to the network (and thus participate in the network's mechanical response) at

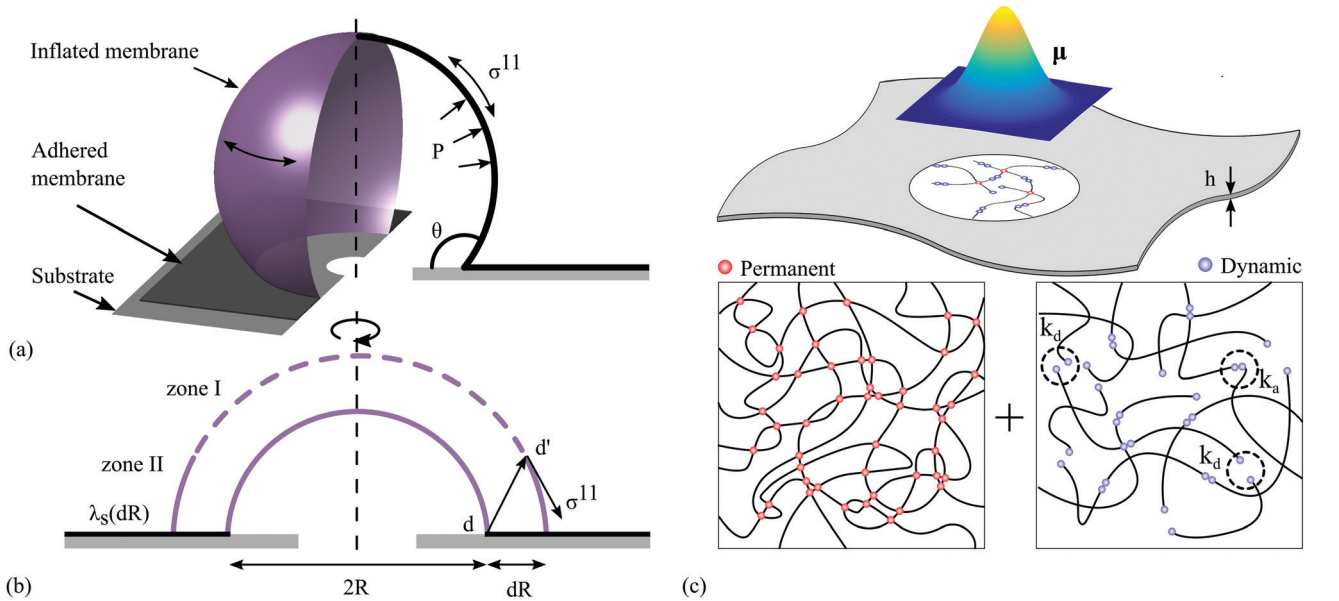

Fig. 1 (a) Scheme of the blister inflation problem. A polymer membrane is attached to a rigid substrate with a circular hole of radius R_0. The injection of a liquid at a rate of $\dot{V}$ creates an internal pressure P, which not only inflates the blister, but also detaches it from the substrate increasing its neck radius R. (b) To determine the variation in the energy release rate during a differential increment in radius dR, the membrane is divided into two zones. Zone I corresponds to a new configuration of the previously detached membrane. Zone II corresponds to the portion of the newly detached membrane, and it is measured by the position vector $\vec{dd}'$. (c) TNT-based schematic of a viscoelastic polymer membrane. The material is assumed to be made of two different types of molecular entanglements. Permanent networks (left) have fixed cross-links, and dynamic networks (right) have transient links attaching and detaching at rates k_a and k_d respectively. Macroscopically, the membrane is described by the statistical distribution of the direction and stretch of the polymer chains which is encapsulated in the tensor $\boldsymbol{\mu}$.

any given time. If the chain dynamics follow first order kinetics, the concentration c of connected chains can be determined at all time by the evolution equation:[39]

$$\dot{c} = k_a(C - c) - k_d c, \tag{3}$$

While the concentration c gives us an indication about the stiffness of the polymer, additional information about the deformation state (and elastic force) of each chain in the network is needed to evaluate the stress state at a point. We have shown in earlier work that this knowledge is encapsulated in the chain distribution tensor $\boldsymbol{\mu}$ (Fig. 1c), whose components indicate the mean squared stretch experienced by the polymer chains in different directions around a material point.[40,41] Thus, if $\boldsymbol{r}$ denotes the end-to-end vector of a chain and $\langle\cdot\rangle$ denotes the average operation over the chain configuration space, $\boldsymbol{\mu}$ is defined by:

$$\boldsymbol{\mu} = \frac{1}{\mathscr{L}b}\langle \mathbf{r} \otimes \mathbf{r} \rangle \tag{4}$$

where $\mathscr{L}$ is the mean chain length and b the Kuhn length. For a membrane, this tensor can be decomposed into tangential ($\boldsymbol{\mu}^t$) and normal ($\boldsymbol{\mu}^n$) components such that $\boldsymbol{\mu} = \boldsymbol{\mu}^t + \boldsymbol{\mu}^n$. Using this decomposition, the evolution of this tensor is captured by two kinetic equations:

$$\dot{\boldsymbol{\mu}}^t = k_a\left(\frac{C-c}{c}\right)\boldsymbol{I} - k_d\boldsymbol{\mu}^t + \boldsymbol{L}\boldsymbol{\mu}^t + \boldsymbol{\mu}^t\boldsymbol{\mu}^T \tag{5a}$$

$$\dot{\mu}^n = \left[k_a\left(\frac{C-c}{c}\right) - k_d\mu^n + 2\frac{\dot{h}}{h}\mu^n\right]\boldsymbol{n}\otimes\boldsymbol{n} \tag{5b}$$

where $\boldsymbol{L}$ is the surface gradient of the tangential velocities, $\boldsymbol{n}$ is the unit normal vector to the mid-plane surface, and μ^n is the normal component such that $\mu^n = \boldsymbol{n}\cdot\boldsymbol{\mu}\cdot\boldsymbol{n}$. In these equations, the first two terms describe the addition of new attached chains (at rate k_a) to the network in a stress-free configuration, and the depletion of previously connected chains (at rate k_d) in their stretched configuration at the time of detachment. The remaining terms describe the change in the chains' average stretch arising from the elastic distortion sustained by the network (under the assumption of affine deformations). Since $\boldsymbol{\mu}$ characterizes the amount of elastic deformation in the network, it can directly be used to estimate the stored elastic energy density. Under the assumption of Gaussian chain statistics, the elastic energy $\Delta\Psi_e$ becomes:

$$\Delta\Psi_e = \frac{ck_BT}{2}\left[\mathrm{tr}\left(\boldsymbol{\mu}^t - \boldsymbol{\mu}_0^t\right) + \left(\mu^n - 1\right)\right], \tag{6}$$

where k_BT is the thermal energy of a molecular chain, and $\boldsymbol{\mu}_0^t$ is the chain distribution tensor when the network is in its stress-free (or natural) configuration. For isotropic materials, such as the VHB tape considered in this paper, $\boldsymbol{\mu}_0^t = \boldsymbol{I}$ where $\boldsymbol{I}$ is the identity tensor. The rate of dissipation $\mathscr{D}$ is then directly related to the elastic energy release rate through chain detachment. It can be shown that:

$$\mathscr{D} = k_d\Delta\Psi_e \tag{7}$$

This form clearly shows that permanent networks ($k_d = 0$) cannot dissipate energy and thus remain purely elastic. The tangent stress tensor $\boldsymbol{\sigma}$ can then be derived using classical thermodynamics[39] to obtain:

$$\boldsymbol{\sigma} = hck_BT(\boldsymbol{\mu}^t - \mu^n\boldsymbol{I}), \tag{8}$$

where we assumed an incompressible polymer membrane.

Eqn (1), (3), (5), and (8) form a general system of equations to describe the mechanical response of a membrane made of a single polymer network whose behavior depends on the values of k_a and k_d. If $k_a = k_d = 0$, the network is said to be permanent, and the polymer behaves elastically as a Neo-Hookean rubber. Otherwise, the network is dynamic, and the polymer exhibits a purely viscous response. In the region of small deformations, this purely viscous response is equivalent to the behavior described by a single Maxwell element. However, the two theories grow apart as the deformation increases, and the Maxwell model loses its accuracy. Although this "single network model" captures the behavior of a viscoelastic material, most polymers display a richer viscoelastic response which can only be explained by the superposition of multiple networks with different dynamic properties. In this situation, each network is described by its distribution tensor $\boldsymbol{\mu}_i$ and the number of attached chain c_i, whose variations are determined by their attachment and detachment rates. For the sake of simplicity, this paper considers a polymer made of two networks: a permanent network with density of attached chains c_0, and a dynamic network with density c_1 and constant rates $k_a = k_d$. These networks are characterized by the fact that the total number c of attached chains remains constant such that:

$$\dot{c} = 0 \quad \Rightarrow \quad k_a\left(\frac{C-c}{c}\right) = k_d, \tag{9}$$

and the tangent stress tensor becomes:

$$\boldsymbol{\sigma} = h\sum_{i=0}^{1} c_i k_B T\left(\boldsymbol{\mu}_i^t - \mu_i^n\boldsymbol{I}\right), \tag{10}$$

In this case, the behavior of the polymer is reminiscent of the standard-linear solid model. The permanent network acts as a purely elastic component with equivalent Young's modulus $E_0 = c_0k_BT/3$, and the dynamic network behaves similarly to a Maxwell element connected in parallel but accounting for finite strains. Hence, introducing the axisymmetric constraints, the stress tensor is simplified to the following two components:

$$\sigma^s = \frac{h}{3}\sum_{i=0}^{1} E_i\left(\mu_i^s - \mu_i^n\right) \quad \sigma^\phi = \frac{h}{3}\sum_{i=0}^{1} E_i\left(\mu_i^\phi - \mu_i^n\right), \tag{11}$$

where $E_i = c_ik_BT/3$. If we consider a time evolution where the membrane moves at a velocity $\boldsymbol{v}$ with tangent component v^s and normal v^n, we can establish the evolution of the axisymmetric distribution tensor as (see Appendix B for details):

$$\dot{\mu}^s = k_d(1-\mu^s) + 2\mu^s(v^s|_s + \kappa_1^1 v^n) \tag{12a}$$

$$\dot{\mu}^\phi = k_d\left(1-\mu^\phi\right) + 2\mu^\phi\left(\frac{r'}{r}v^s + \kappa_2^2 v^n\right) \tag{12b}$$

$$\dot{\mu}^n = k_d(1-\mu^n) + 2\frac{\dot{h}}{h}\mu^n \tag{12c}$$

2.3 Delamination mechanics of a viscoelastic membrane

The adhesion energy between the blister and its substrate is measured by the energy release rate G that characterizes the energy dissipated during the detachment of a unit membrane area. While an expression for G was previously derived for an elastic blister undergoing finite deformation by Long *et al.*,[26] the case of a visco-elastic blister differs by the fact that dissipation originates from (a) the viscous deformation of the membrane and (b) the loss of adhesion energy. To quantify these contributions, the energy release rate is first expressed in terms of the adhesion energy Γ, and the delamination area A as:

$$G = -\lim_{dA\to 0}\frac{\delta\Gamma}{dA} \tag{13}$$

The adhesion energy is then assessed by considering the energy balance during the detachment of a differential portion of the membrane from its substrate under the action of the blister's internal pressure. During this process, the rate of mechanical work done by the pressure is equal to the sum of the viscous dissipation occurring in the initially detached membrane (zone 1 in Fig. 1b) and the change in adhesion energy $\delta\Gamma$ resulting from the detachment of a differential portion dR (zone 2 in Fig. 1b). The latter can be expressed as the difference between the external and internal energies as:

$$\delta\Gamma = (\delta U_e + \delta U_d) - \delta W_p \tag{14}$$

where δW_p is the work done by the applied pressure on the entire system, δU_e is the change in the membrane's elastic energy, and δU_d is the viscous dissipation. Assuming then that there is no slip in the contact region, this energy can be split into zones I and II, *i.e.* $\delta\Gamma = \delta\Gamma^I + \delta\Gamma^{II}$, where each term corresponds to their own contributions $(\delta U_e^\alpha + \delta U_d^\alpha) - \delta W_p^\alpha$ (α = I, II).

Zone I. We can equate the internal energy $(\delta U_e^I + \delta U_d^I)$ in zone I to the work done by external forces, which include the work done by the internal pressure δW_p^I and the work $2\pi R\vec{\sigma}\cdot\vec{dd'}$ done by the line tension $\vec{\sigma}$ to bring point d to d' (Fig. 1b).

For a differential displacement in an axisymmetric blister, we can write the line tension as a function of the contact angle θ (Fig. 1b) and the longitudinal stress at the delamination point $\vec{\sigma} = -\sigma^s(\hat{e}_r\cos\theta + \hat{k}\sin\theta)$. Similarly, following the scheme of Fig. 1b, the displacement vector can be written as $\vec{dd'} = (dR')(\hat{e}_r\cos\theta + \hat{k}\sin\theta) - (dR)\hat{e}_r$, where dR' corresponds to the new detach material points after deformation; *i.e.*, $dR' = \lambda_s dR$, λ_s being the stretch at the onset of delamination. Thus, the contribution of the total energy in zone I takes the form:

$$\delta\Gamma^I = 2\pi R\sigma^s(\cos\theta - \lambda_s)dR \tag{15}$$

Zone II. First, because zone II has an infinitesimal surface area, the change in volume in this region is of the order of $2\pi R\delta R|dd'|$ and scales with dR^2. Consequently, since the work

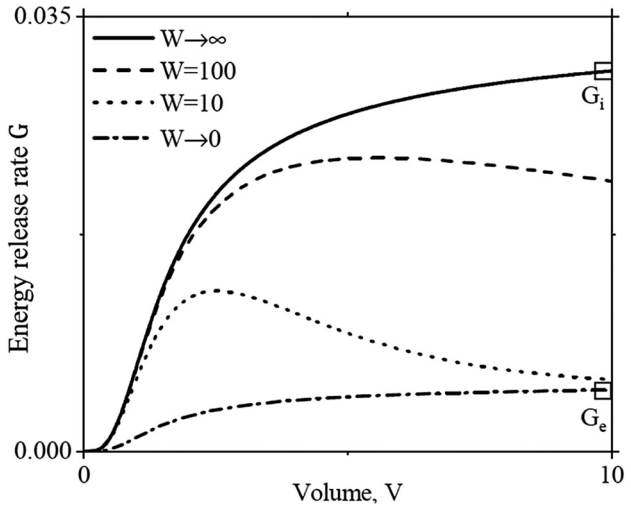

Fig. 2 Evolution of the nondimensional energy release rate G^* with the nondimensional blister volume V^* at four different inflation speeds (W = 0, 5×10^2, 5×10^3, and ∞) and for a constant neck R^* = 7. For quasistatic inflation rates ($W \to 0$), the blister has an elastic growth such that G^* exhibits an asymptotic behavior with upper limit G_e. The same behavior is observed in extremely fast inflations ($W \to \infty$), where the blister has an elastic behavior governed by an instantaneous elastic modulus E_i which sets an upper limit G_i.

of pressure δW_p^{II} is proportional to this change in volume, it can be neglected due to the presence of a double differential.[26] Second, the dissipated energy in this zone is $\delta U_d^{II} = \mathscr{D} dV^{II} dt$, with volume $dV^{II} = 2\pi R h \lambda_s dR$. Again, the presence of a double differential ($dR dt$) allows us to neglect this contribution to the total energy. The stored elastic energy is, however, non-negligible and can be derived using eqn (4) as $\delta U_e^{II} = dV^{II} \Delta\Psi_e^d$, where $\Delta\Psi_e^d$ is the stored elastic energy density at the delamination point. Hence, we can write the contribution of part II to the total adhesion energy as:

$$\delta\Gamma^{II} = 2\pi R h \lambda_s dR \Delta\Psi_e^d. \quad (16)$$

Energy release rate. The energy release rate G can then be found by substituting the results of eqn (15) and (16) into expression (13), where $\delta\Gamma = \delta\Gamma^{I} + \delta\Gamma^{II}$. We find:

$$G = -\frac{1}{2\pi R} \lim_{dR \to 0} \left(\frac{\delta\Gamma}{dR} \right) = \sigma_d^s (\lambda_s - \cos\theta) - h\lambda_s \Delta\Psi_e^d \quad (17)$$

There are two main differences between this result and the expression provided by Long *et al.*[26] for the elastic case. (i) The value of the stresses and elastic energies are time-dependent, and consequently, they must be integrated in time. (ii) The second term is a function of the current thickness h and the elastic energy density per current volume $\Delta\Psi_e$, instead of being a function of the initial reference state of the membrane. This is a consequence of the fact that dynamic networks have no shape memory and TNT is derived in the current frame of reference.

3 Blister mechanics at constant neck radius

To understand how blister inflation potentially affects delamination, we first present results regarding the inflation of a blister with constant neck radius. For generality, we first nondimensionalized the problem by introducing the following variables:

$$R^* = \frac{R}{h_0} \quad V^* = \frac{V}{h_0^3} \quad G^* = \frac{G}{E_0 h_0}, \quad W = \frac{\dot{V}}{h_0^3 k_d} \quad (18)$$

where R^* is the nondimensional neck radius of the blister, V^* its nondimensional volume, G^* is the nondimensional energy release rate, and W the Weissenberg number that captures the competition between the inflation rate and viscous dissipation in the membrane.

3.1 Effect of the inflation rate on the energy release rate

Stresses in viscoelastic membranes are sensitive to their rate of deformation; larger loading rates typically yield larger stresses. This means that the energy release rate, which eventually controls the onset of delamination, is likely to be sensitive to the inflation rate of a blister. To explore this hypothesis, we consider a blister, characterized by a constant neck radius R^* = 7 and determine the relation between G^* and blister volume V^* for different volume inflation rates (Fig. 2). We observe that, for quasistatic inflation ($W \to 0$), the viscous forces vanish and G^* increases with inflation until it reaches an asymptotic value G_e^*. This observation may be explained by the fact that G^* is proportional to the longitudinal stress σ^s, which has a similar asymptotic behavior during the inflation of spherical membranes.[42] When the blister is inflated at very large rates ($W \to \infty$), the dynamic network does not have time to relax, and the membrane is endowed with an elastic modulus $E_I = (c_0 + c_1) k_B T$ that consists of the combined permanent and dynamic networks. As a result, we observe a behavior that is very similar to that for slow inflation, but with a larger asymptotic energy release rate G_i^*. In general, for a constant neck radius R^*, the energy release rate will always be bounded between its lower and upper limits G_e^* and G_i^*, respectively. For intermediate inflation rates, however, the competition between elasticity and dissipation leads to a nonlinear response where G^* exhibits a local maximum, after which the energy release rate monotonically decreases with blister volume. We note that this response is directly related to the nonlinear pressure–volume relation and elastic instability observed in soft spherical membranes,[36] where the inflation pressure exhibits a maximum as its radius increases 38% its initial value. This response, previously discussed in ref. 43 and 44, has important consequences when the membrane is allowed to delaminate as shown in the following section. It is important to note that none of the blisters modeled in this paper has a perfectly spherical shape. In the case of purely neo-Hookean rubbers, Long *et al.*[26] demonstrated that these differences are small enough such that theories based on purely spherical geometries[45] might lead to accurate and insightful results.

Despite the presence of a viscous component, the same behavior was observed with our constitutive model where the blisters only showed a noticeable deviation from a purely spherical shape when $\theta < \pi/2$. These comparisons might however lose their accuracy on more complex behaviors (*i.e.*, strain stiffening or nonlinear chain dynamics).

3.2 A phase diagram for delamination

In order to study these concepts in a broader parameter space, let us now consider the inflation of an initially flat blister at a constant volume rate W and neck radius R^*. Due to the incompressibility of the filling liquid, the delamination of a blister can be characterized by the variation of G^* within the $V^* - R^*$ space (Fig. 3a). Indeed, each $V^* - R^*$ pair defines a unique blister profile (or shape) whose stability is inferred by the relation between the energy release rate G^* (also interpreted as the driving force for delamination) and a critical value G_0^* ($G_0^* = G_0/E_0h$) at which delamination occurs. Thus, if $G^* > G_0^*$, delamination takes place and the adhesion is said to be unstable; by contrast, if $G^* < G_0^*$, the blister neck remains constant, and the adhesion is said to be stable. The intersection between this surface and the plane $G^* = G_0^*$ defines a phase diagram delimiting the stable and unstable regions (Fig. 3b).

We have previously found that the adhesion energy has an upper bound G_i^* for each value of R^*. This implies that if G_0^* is high enough, the blister is permanently stable and unable to delaminate regardless of the inflation speed. However, as the value of G_0^* decreases, the phase diagram shows a closed unstable region. Considering the inflation of a blister with zero initial volume, two main conclusions can be extracted from this result. (i) For each value of G_0^* there is a minimum R^* above which the blister always remains stable independently of its volume. (ii) If the neck radius is constrained, it is possible that the adhesion energy might eventually drop below the adhesion threshold, leaving the blister stable. In other words, the blister is trapped (it does not spread) despite having a higher liquid volume. This is not the case when $G_0^* < G_e^*$ since the blister always remains unstable at higher volumes and will eventually delaminate.

While the information provided by the phase diagram of Fig. 3b is useful to understand the adhesive stability of a blister, G_0^* is a fixed property depending on the affinity between the membrane and the substrate, which is generally hard to control. Instead, most systems are driven by the volume rate $\dot{V}$, or equivalently, the Weissenberg number W, and have a fixed adhesion threshold. In terms of the phase diagram, varying the Weissenberg number implies that our plane $G^* = G_0^*$ remains fixed, and it is the entire surface that changes according to the results shown in Fig. 2. Hence, we obtain a particular phase diagram (Fig. 4) where each contour in the $V^* - R^*$ space defines two stability regions whose shape depends on the inflation rate $\dot{V}$. As discussed before, the adhesion energy during an extremely fast inflation ($W \to \infty$) has an increasingly asymptotic behavior acting as an upper bound of the system. In this phase diagram, this particular case creates two main regions (Fig. 4). (1) A permanently stable region which is completely independent of the inflation rate; *i.e.*, the blister would never delaminate under those $V^* - R^*$ conditions. (2) A potentially unstable region where delamination depends on the inflation rate. Indeed, as the inflation rate decreases, we observe how the stability regions become a closed loop in the phase diagram such that the blister would only delaminate when its $V^* - R^*$ state falls within the loop. Finally, in cases where $G_0^* > G_e^*$, there is a lower threshold on W where the stresses never increase enough to break the adhesive bonds, and the blister remains stable during the entire inflation process.

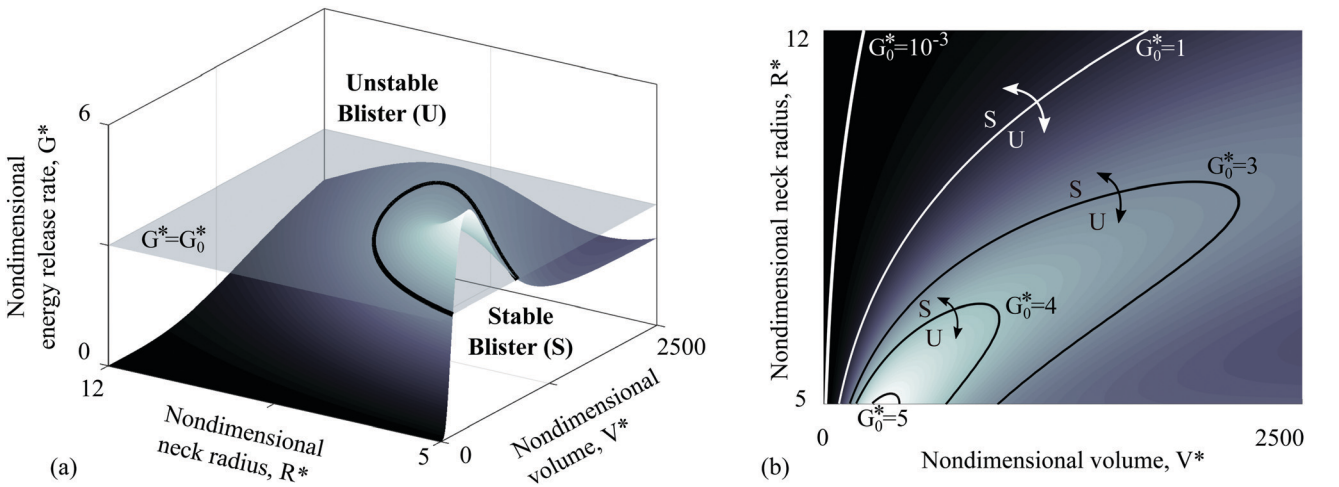

Fig. 3 (a) Nondimensional adhesion energy as a function of its neck radius and liquid volume for a blister inflated at a constant volume rate (W = 500). The surface is cut by a flat plane ($G^* = G_0^*$) dividing the surface into two main regions: stable blisters with no delamination ($G^* < G_0^*$) and unstable blisters that delaminate ($G^* > G_0^*$). (b) Phase diagram built from (a) where the color shows the value of the adhesion energy as a function of the neck radius R^*, and the volume V^*. The different lines show the limits of the stability regions (stable (S) and unstable (U)) resulting from having different values of G_0^*. Note that as $G_0^* \to 0$ the unstable region grows until it spans the entire space. On the other end of the spectrum, if $G_0^* \to \infty$ the unstable region shrinks until it vanishes at $G_0^* > G_{max}$, and the blister is stable at every $R^* - V^*$ configuration.

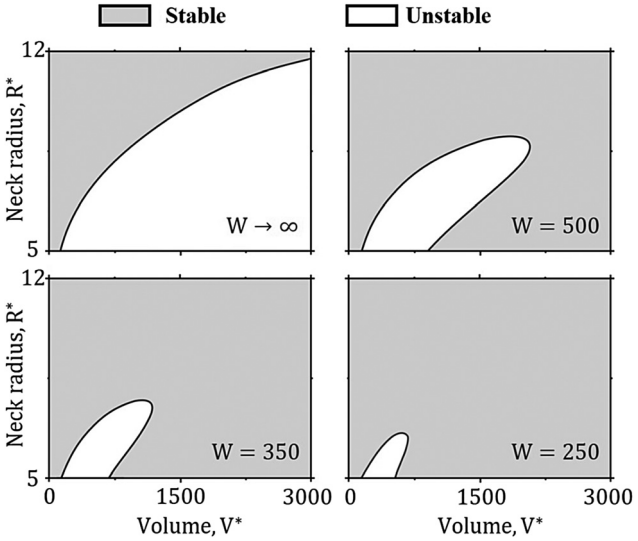

Fig. 4 Stability phase diagram $V^* - R^*$ obtained at a constant adhesion threshold G_0^* but for different values of the Weissenberg number, namely $W = 250$, $W = 350$, $W = 500$, and $W \to \infty$. The shaded region corresponds to a permanently stable adhesion; *i.e.*, the blister is stable regardless of the inflation rate, and corresponds to the upper bound of the system obtained at $W \to \infty$. The rest of the diagram corresponds to a potentially unstable adhesion depending on the inflation rate. Each value of W defines a different limit such that the blister configuration is unstable inside the white region and stable in the gray region.

4 Dynamics of blister growth

Let us now concentrate on the case where the blister is allowed to delaminate and spread during inflation. This necessitates the introduction of a new time scale that governs the typical delamination rate of a membrane on a substrate. Indeed, if the spreading velocity is significantly larger than the inflation rate, one may expect a flat blister that grows by spreading on its substrate. By contrast, when the inflation rate is significantly faster than the rate of delamination, the blister will mostly grow in height.

4.1 A simple model of blister spreading

Delamination dynamics have been extensively studied in the literature, and the evolution of the neck ($\dot{R}$) is well-captured by the following empirical relation:[46]

$$\dot{R} = \begin{cases} 0 & \text{if} \quad G < G_0 \\ v\left(\dfrac{G}{G_0} - 1\right)^{\frac{1}{n}} & \text{if} \quad G \geq G_0 \end{cases} \tag{19}$$

where v is the critical velocity at which the effect of viscous dissipation at the crack tip becomes important, while n is the adhesion exponent and depends on the properties of the substrate/membrane pair. In this work, the latter value is taken as $n = 2$ following the adhesion mechanics of PDMS.[35]

In the above static analysis, we showed that the phase diagrams of Fig. 4 allow for a stability classification of any blister defined by a $V^* - R^*$ pair. However, this information is not sufficient to establish its inflation history. In fact, this question may be answered by rewriting (19) in a way that it describes the path taken by an inflating blister in the $R^* - V^*$ plane. It is indeed straightforward to show that:

$$\dot{\boldsymbol{x}} = \begin{Bmatrix} \dot{R}^* \\ \dot{V}^* \end{Bmatrix} = \begin{Bmatrix} \dot{R}^*(v^*, G^*) \\ W \end{Bmatrix}, \tag{20}$$

where $\dot{R}$ is given by eqn (19), and $v^* = v/k_d h_0$. This system of differential equations can be directly integrated in cases where there is no inflation ($\dot{V} = 0$), or no delamination ($G < G_0 \Rightarrow \dot{R} = 0$). Otherwise, one must use the relationship between the delamination velocity and the volume as $\dot{R} = \dot{V}\mathrm{d}R/\mathrm{d}V$ where $\dot{V} = W h_0^3 k_d$. Substituting this result in eqn (20), one obtains a single differential equation that governs the dynamics of blister growth when inflation and delamination coexist:

$$W\frac{\mathrm{d}R^*}{\mathrm{d}V^*} = \frac{v}{h_0 k_d}\left(\frac{G}{G_0} - 1\right)^{\frac{1}{n}}, \tag{21}$$

This equation can be numerically integrated given the initial volume V_0^*, neck R_0^*, and Weissenberg number W to determine the time evolution of blister growth. In summary, the solution consists of two branches: when the blister is in the stable region ($G^* < G_0^*$), there is no delamination and the blister grows at constant R following a horizontal path in the phase diagram. Alternatively, when a blister is in the unstable region ($G^* > G_0^*$) delamination occurs and the blister neck grows at a rate given by (21).

4.2 Blister spreading dynamics and trapping

Before analyzing predictions for the model, we first note that the problem is now driven by the interplay of three length-scales: the relaxation time of the polymer, the inflation (volume) rate, and the delamination time (captured by the intrinsic speed v^*). For clarity, we thus limit our analysis to constant inflation rates W and introduce the spreading coefficient $Z = W/v^*$ to capture the competition between inflation and delamination rates. Fig. 5 shows blister trajectories predicted by the model for three values of Z ($Z \to 0$, $Z = 2 \times 10^3$, and $Z = \to \infty$). Initially, all blisters start in a stable domain, *i.e.*, no delamination takes place ($V^* = 0$), and they follow a horizontal path in the $V^* - R^*$ space. Once the blisters reach the unstable domain, however, delamination starts and the blister paths, which depend on inflation rates, diverge. We discuss below the characteristics of these paths in three situations.

Slow inflation ($Z \to 0$). When the dynamics of delamination are much faster than the inflation rate, blisters are unable to penetrate the unstable domain and remain on its boundary (Fig. 5a). In other words, the blister first follows a horizontal path (no delamination) until it meets the boundary of the unstable domain. At this point, its path follows this boundary, since it maximizes neck spreading for all inflation volumes. If the unstable domain is bounded, the blister eventually reaches a maximum neck radius, after which it is unable to delaminate further and retrieve a horizontal path. Depending on the adhesion energy, the outcome will be a relatively flat blister ($\theta < \pi/2$) that maximizes its neck size. We finally note

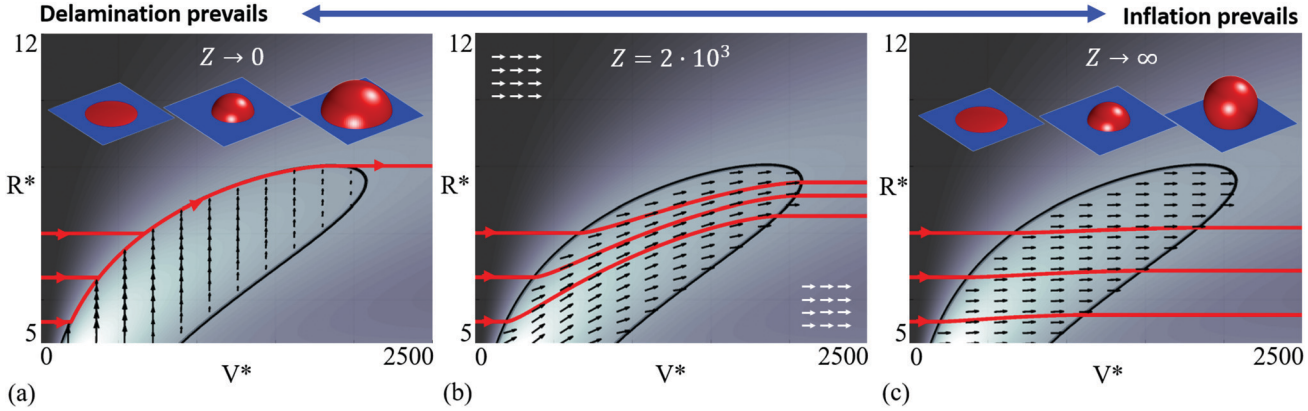

Fig. 5 $R^* - V^*$ path followed by three blisters with initial radii R^* = 6, 8, and 10, which are inflated at a constant Weissenberg number (W = 500). The three scenarios (a–c) show the effect of varying the spreading coefficient $Z = W/v^*$, which corresponds to having blisters with different spreading velocities. (a) A case where $Z \to 0$ such that $v^* \gg$ W. In this scenario, blister delamination prevails over blister inflation. The blisters are unable to penetrate the unstable regime, and the path follows the boundary between the two regions. (b) An intermediate case (Z = 2000) where the blisters penetrate the unstable domain and progressively delaminate until G drops again below the threshold G_0. Finally, (c) shows the case inflation prevailing over delamination ($Z \to \infty$). Under these conditions, the blisters enter and exit the unstable regime fast enough such that their neck radius remains almost the same. Indeed, despite the high volume and stresses in the system, the relaxation rate can lower the energy release rate below the threshold before the blisters have time to delaminate significantly.

that if a blister initially starts within the unstable domain, it will first follow a vertical path (*i.e.*, it will delaminate before growing). These paths are indicated with vector fields in Fig. 5.

Fast inflation ($Z \to \infty$). When inflation is significantly faster than the blister's spreading dynamics, the rate of neck growth becomes negligible compared to the rate of volume growth. We thus observe growth in volume at quasi-constant neck size, as depicted by the horizontal paths in Fig. 5c. Interestingly, this condition allows a blister to cross-over the unstable domain without spreading (as represented by the horizontal vector fields) and eventually become stable once they are large enough. The outcome will be a large and stable quasi-spherical blister with a small neck radius.

Intermediate inflation rates. Blisters inflated at relatively moderate rates are able to enter the unstable domain, in which they experience a combination of inflation and delamination, depending on the value of the spreading coefficient Z. Fig. 5b shows three typical paths taken by blisters, with different initial neck radii, subjected to $Z = 2 \times 10^3$. Overall, a blister possesses three stages of growth: (a) growth without delamination until it reaches the unstable domain, (b) combined inflation and spreading, whose ratio depends on the value of Z and (c) return to a stable stage, where the blister grows without spreading. In this case, the blister is trapped at a higher volume, *i.e.*, it will never delaminate again past this point. While our study only considered constant inflation rates W, it is worth noting that stopping the inflation in the unstable domain would force the blister to follow vertical growth until it reaches the boundary between stable and unstable zones. In this case, a blister would not necessarily reach a maximum neck radius.

4.3 Experimental test

To observe these predictions in a simple experiment, we designed a blister test using a hyperelastic adhesive tape (VHB 4905) adhered to an aluminum substrate and inflated at a constant volume rate. Since the tape and its adhesion both exhibit complex viscoelastic response,[44,47] whose study is beyond the scope of our work, our objective here is not to quantitatively match modeling results, but rather to qualitatively demonstrate the key concepts developed in this study (*i.e.* observe rate-dependent blister growth, spreading and trapping).

Our experimental setup consists of an aluminum plate with a circular hole of radius R_0 = 3.5 mm perfectly attached to a 3D-printed base. This piece enabled connecting the hole to a NE-1000 syringe pump (NEWERA Pump Systems Inc.) using a set of polyethylene tubes. In order to inflate a blister, we then attached a piece of VHB 4905 (h_0 = 0.5 mm) on top of the aluminum board and injected dyed water at a constant volume rate $\dot{V}$. Since the thickness (h_0) and the mechanical parameters (k_d, and c_i) of the adhesive tape were set by the manufacturer, we only had control over two of the four nondimensional parameters: R^* and W. Since the manufacturer sets the thickness of the tape, the former parameter (R^* = 7) is controlled by modifying the radius of the circular hole in the aluminum plate. The Weissenberg number W was controlled *via* the volume rate $\dot{V}$. Although the relaxation of VHB possesses multiple relaxation times,[44] its chain dynamics is approximated by an average value $k_d \approx 0.0028\ 1/s$[44] which establishes an operational range of W between 3 and 3×10^4. The rest of the nondimensional parameters, G^* and v^*, are unknowns which depend on the contact properties between VHB and aluminum and which would need to be calibrated. Furthermore, as described by the manufacturer, the adhesion strength of the VHB tape is not reached instantaneously, and it takes around 72 hours to reach its maximum potential. At this stage, we observed that the pressure induced by the inflation of a blister was not enough to delaminate the membrane; *i.e.*, $G_0 \gg G_i$. To counter this effect, we performed all blister tests exactly 5 minutes after the tape was attached to the aluminum plate.

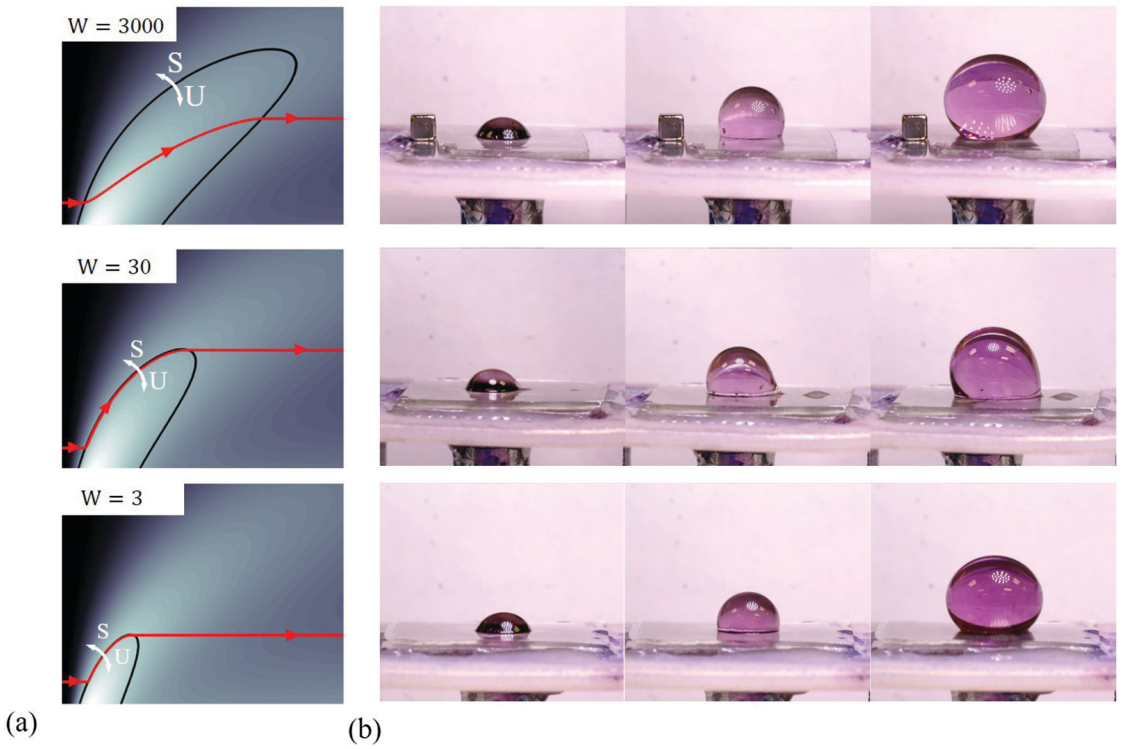

Fig. 6 (a) Evolution of three blisters with an identical initial state (v^*, R^*), but which are inflated at three different volume rates (W = 3, 30, 3000) such that the fastest inflation does not yield the fastest spreading. (b) Experimental observations of three different blisters inflated at different rates namely $\dot{V}$ = 0.1, 1, and 10 ml min^{-1}. Assuming a constant value of k_d = 0.00281 s^{-1}, these values correspond to effective Weissenberg numbers of the order of W = 3, 30 and 3000.

At this moment, we observed that the level of adhesion G_0 was on the same scale as the energy release rate G induced by the stresses on the membrane. Hence, this ensured to have a low enough adhesion such that the blister would delaminate with the incoming water and allowed us to investigate the different scenarios previously described in this paper.

Using this experimental setup, Fig. 6b shows the results of the resulting blister growth at three inflation rates: 0.001 ml min^{-1}, 0.1 ml min^{-1}, and 10 ml min^{-1}, which would correspond to Weissenberg numbers on the order of 3, 30, and 3000. We observe that the blisters inflated at faster and slower rates have similar profiles. In the slowly inflated blister, this phenomenon occurs due to the fact that the viscous forces are very low and $G < G_0$. If we stopped inflating, its radius would remain the same. By contrast, for the quickly inflated blister, a similar profile due to the blister has not had enough time to delaminate, indicated by the higher values of Z. If we stopped inflating, its radius would continue to grow. For the intermediate case, however, we observe the highest spreading dynamics as the blister is inflated at a rate where W and v^* are comparable. This results in a larger neck radius compared to the other two cases.

5 Conclusions

In this paper, we presented a new model combining the transient network theory (TNT) and adhesion mechanics under finite deformation to study the mechanics of a viscoelastic blister. We found that the combination of a hyperelastic rubber with highly viscous properties yields a nonlinear behavior of the adhesion energy with a new adhesive instability not present with pure elasticity. For instance, we show that the blister stability is not only determined by its geometry, but also by its inflation rate. Our results suggest that this problem can be well understood from the phase diagram where the adhesion energy is plotted as a function of the neck radius and blister volume. This approach was used to demonstrate that the final shape of a blister can be highly controllable by tuning the initial neck radius, membrane thickness, or inflation rate. Nonetheless, there are still many parameters such as the pre-stretch of the membrane,[33] or the slippage during delamination[48] whose effect in combination with membrane viscosity remains unknown. In addition, TNT not only allows for an easy adaptation to other viscous materials, but it also opens the door to future exploration on how specific material properties might affect the behavior of blisters. For example, considering more realistic non-constant values for the crosslink density or the attachment and detachment rates will undoubtedly have profound implications on the conclusions drawn in this manuscript.

Being able to control the morphology of a surface is a crucial feature in many processes such as adhesion, friction, camouflage, or hydrophobicity of materials. For instance, blister-like actuators made of hydrogels[49] or dielectric materials[50] rely on the rubber instability in order to achieve extreme blister-like

deformations. However, this instability, as well as the potential delamination of the material, depends on its viscous properties, which so far have not been studied. In addition, the combination of the problem considered here with novel reversible adhesion techniques[51,52] would provide an ideal framework to achieve a controllable and reversible shape morphing material similar to the one shown by arthropods. For this, one should also consider the effect of damage in the network due to large deformation on the mechanical response.[53]

Conflicts of interest

There are no conflicts to declare.

Appendix A: membrane mechanics

In order to derive the governing equations of a membrane, we start by parametrizing its position in space. As discussed in the main text, the slenderness of a membrane allows representing it by a 2D surface, the mid-plane, embedded in a 3D space. This surface can be parametrized as $\boldsymbol{x} = \boldsymbol{x}(\xi^1,\xi^2)$, where ξ^α are the parametric coordinates. Hence, we can define a local coordinate system made of two tangent vectors $\boldsymbol{a}_\alpha = \boldsymbol{x}_{,\alpha}$ and a normal to the mid-plane $\boldsymbol{n} = \boldsymbol{a}_1 \times \boldsymbol{a}_2/\|\boldsymbol{a}_1 \times \boldsymbol{a}_2\|$. In this coordinate system, a vector and a tensor are written respectively as:

$$\boldsymbol{v} = v^\alpha \boldsymbol{a}_\alpha + v^n \boldsymbol{n} \tag{22}$$

$$\begin{aligned}\boldsymbol{\sigma} \;=\; & \underbrace{\sigma^{\alpha\beta}\boldsymbol{a}_\alpha \otimes \boldsymbol{a}_\beta}_{\boldsymbol{\sigma}^t} + \sigma^{\alpha n}\boldsymbol{a}_\alpha \otimes \mathbf{n} \\ & + \sigma^{n\beta}\boldsymbol{n} \otimes \boldsymbol{a}_\beta + \underbrace{\sigma^n \boldsymbol{n} \otimes \boldsymbol{n}}_{\boldsymbol{\sigma}^n}\end{aligned} \tag{23}$$

In addition to this, we can define the metric tensor of the surface in its covariant form as $a_{\alpha\beta} = \boldsymbol{a}_\alpha \cdot \boldsymbol{a}_\beta$, which provides mapping between the parametric space and the actual representation of the membrane. This tensor can alternatively be represented in its contravariant form as $a^{\alpha\beta}$ defined by $a^{\alpha\beta}a_{\beta\gamma} = \delta^\alpha_\gamma$. Finally, the representation of a membrane is closed by defining the curvature tensor in both its covariant and mixed forms respectively by:

$$\kappa_{\alpha\beta} = \boldsymbol{a}_{\alpha,\beta} \cdot \boldsymbol{n} \;\; \kappa^\alpha_\beta = a^{\alpha\gamma}\kappa_{\gamma\beta} \tag{24}$$

These local curvilinear coordinate systems are generally characterized by the fact that they are not orthonormal. This implies that one must redefine the variations in tensor by taking into account the variation of both the components and the basis. Hence, we can write the divergence and gradient of a vector and a tensor respectively as:

$$\nabla \cdot \boldsymbol{v} = (v^\alpha|_\beta) \tag{25a}$$

$$\nabla \cdot \boldsymbol{\sigma} = (\sigma^{\alpha\beta}|_\beta)\boldsymbol{a}_\alpha \tag{25b}$$

$$\nabla \boldsymbol{v} = (v^\alpha|_\beta)(\boldsymbol{a}_\alpha \otimes \boldsymbol{a}^\beta) \tag{25c}$$

$$\nabla \boldsymbol{\sigma} = (\sigma^{\alpha\beta}|_\gamma)(\boldsymbol{a}_\alpha \otimes \boldsymbol{a}_\beta \otimes \boldsymbol{a}^\gamma) \tag{25d}$$

where the vertical bar indicates a covariant derivative:

$$v^\alpha|_\beta = v^\alpha_{,\beta} + \Gamma^\alpha_{\beta\gamma}v^\gamma \tag{26a}$$

$$\sigma^{\alpha\beta}|_\gamma = \sigma^{\alpha\beta}_{,\gamma} + \Gamma^\alpha_{\mu\gamma}\sigma^{\mu\beta} + \Gamma^\beta_{\gamma\mu}\sigma^{\alpha\mu} \tag{26b}$$

and $\Gamma^\alpha_\alpha = \frac{1}{2}a^{\alpha\mu}\left(a_{\beta\mu,\gamma} + a_{\gamma\mu,\beta} - a_{\beta\gamma,\mu}\right)$ are the Christoffel symbols. The equilibrium equations of a shell in this curvilinear basis are determined by introducing these definitions into the balance of linear and angular momentum such that one obtains:

$$\sigma^{\alpha\beta}|_\beta + f^\alpha = 0 \tag{27}$$

$$\sigma^{\alpha\beta}\kappa_{\alpha\beta} + f^n = 0 \tag{28}$$

Appendix B: axisymmetric details

In this appendix, we carry out the mathematical conditions to obtain the axisymmetric form of the equations to finally obtain the equations in an implementation-ready form. Let us start by introducing the following polar parameterization on the mid-plane:

$$\boldsymbol{\varphi} = [r(\xi^1)\cos\xi^2, r(\xi^1)\xi^1\sin\xi^2, z(\xi^1)] \tag{29}$$

By simply applying the definitions of Appendix A, we can write the metric tensor as:

$$a_{\alpha\beta} = \begin{bmatrix} r'^2 + z'^2 & 0 \\ 0 & r^2 \end{bmatrix} \tag{30}$$

where we used $'$ to indicate a derivative with respect to ξ^1. In a similar way, the only non-zero Christoffel symbols can be written as:

$$\Gamma^1_{11} = \frac{r'r'' + z'z''}{a_{11}} \quad \Gamma^1_{22} = -\frac{rr'}{a_{11}} \quad \Gamma^2_{21} = \frac{r'}{2} \tag{31}$$

and thus we can write the membrane equations as:

$$\sigma^{11}_{,1} + (2\Gamma^1_{11} + \Gamma^2_{21})\sigma^{11} + \Gamma^1_{21}\sigma^{22} + \dot{f}^1 = 0 \tag{32a}$$

$$\sigma^{11}\kappa_{11} + \sigma^{22}\kappa_{22} + f^n = 0 \tag{32b}$$

Next, if we consider the real stress in the shell by taking into account the magnitude of the basis, we can redefine the true stresses on the membrane in its longitudinal and hoop directions respectively as:

$$\sigma^s = \sigma^{11}a_{11} \quad \sigma^\phi = \sigma^{22}a_{22}, \tag{33a}$$

and substituting both (31) and (33) into (32) we directly obtain the simplified form of the balance of linear momentum shown in eqn (2). Similarly, to obtain the simplified forms of the distribution tensor, we start by expressing the velocity gradient $\boldsymbol{L} = \nabla\mathbf{v}$ in terms of local basis as:[44]

$$\begin{aligned}\mathbf{L} \;=\; & \left(v^\alpha|_\beta - v^n\kappa^\alpha_\beta\right)(\mathbf{a}_\alpha \otimes \mathbf{a}^\beta) + \left(v^\gamma\kappa_{\gamma\beta} + v^n_\beta\right)(\mathbf{n} \otimes \mathbf{a}^\beta) \\ & + \frac{\dot{h}}{h_0}\mathbf{n} \otimes \mathbf{a}^3 - \frac{h}{h_0}\left(v^\alpha\kappa_{\alpha\beta} + v^n_{,\beta}\right)\alpha^\beta \otimes \mathbf{a}^3.\end{aligned} \tag{34}$$

Then, by plugging this expression into eqn (5a) and (5b), and noting that $v^{\phi}|_{\phi} = v^{s}/r$ for the axisymmetric condition, we can obtain the expression of eqn (12a)–(12c):

$$\dot{\mu}^{s} = k_{d}(1 - \mu^{s}) + 2\mu^{s}(v^{s}|_{s} + \kappa_1^1 v^{n}) \quad (35a)$$

$$\dot{\mu}^{\phi} = k_{d}(1 - \mu^{\phi}) + 2\mu^{\phi}\left(\frac{r'}{r}v^{s} + \kappa_2^2 v^{n}\right) \quad (35b)$$

$$\dot{\mu}^{n} = k_{d}(1 - \mu^{n}) + 2\frac{\dot{h}}{h}\mu^{n}. \quad (35c)$$

Acknowledgements

We acknowledge Tong Shen's help in reviewing the manuscript. Research reported in this publication was supported by the National Science Foundation under the award 1761918. The content is solely the responsibility of the authors and does not necessarily represent the official views of the National Science Foundation.

References

1 J. Nardi, T. Feder, R. Bruinsma and E. Sackmann, *Europhys. Lett.*, 1997, **37**, 371–376.
2 K. T. Wan and Y. W. Mai, *Acta Metall. Mater.*, 1995, **43**, 4109–4115.
3 Y. Aoyanagi, J. Hure, J. Bico and B. Roman, *Soft Matter*, 2010, **6**, 5720–5728.
4 N. G. Boddeti, S. P. Koenig, R. Long, J. Xiao, J. S. Bunch and M. L. Dunn, *J. Appl. Mech.*, 2013, **80**, 040909.
5 T. Zhu, G. Li, S. Müftü and K.-T. Wan, *J. Appl. Mech.*, 2017, **84**, 071005.
6 M. Nase, B. Langer and W. Grellmann, *Polym. Test.*, 2008, **27**, 1017–1025.
7 M. Nase, B. Langer, H. J. Baumann, W. Grellmann, G. Geißler and M. Kaliske, *J. Appl. Polym. Sci.*, 2019, **111**, 363–370.
8 I. Starnberger, D. Preininger and W. Hödl, *Anim. Behav.*, 2014, **97**, 281–288.
9 J. J. Allen, G. R. Bell, A. M. Kuzirian, S. S. Velankar and R. T. Hanlon, *J. Morphol.*, 2014, **275**, 371–390.
10 L. Foucard, X. Espinet, E. Benet and F. J. Vernerey, *Multi-scale Simulations and Mechanics of Biological Materials*, 2013, pp. 241–265.
11 F. J. Vernerey and M. Farsad, *Comput. Meth. Biomech. Biomed. Eng.*, 2011, **14**, 433–445.
12 G. T. Charras, M. Coughlin, T. J. Mitchison and L. Mahadevan, *Biophys. J.*, 2008, **94**, 1836–1853.
13 A. Srivastava, A. B. Tepole and C. Y. Hui, *Extreme Mech. Lett.*, 2016, **9**, 175–187.
14 A. Patil and A. Dasgupta, *European Journal of Mechanics, A: Solids*, 2013, **41**, 28–36.
15 J. A. Rodríguez-Martínez, J. Fernández-Sáez and R. Zaera, *Int. J. Eng. Sci.*, 2015, **93**, 31–45.
16 A. Libai and J. Simmonds, *The nonlinear theory of elastic shells*, 1988, p. 428.
17 A. E. Green and W. Zerna, *Theoretical Elasticity*, Courier Corporation, 2002, p. 457.
18 A. Derdouri, F. Erchiqui, A. Bendada, E. Verron and B. Peseux, *Proceedings of the International Congress on Rheology, 13th, Cambridge, United Kingdom, Aug. 20–25, 2000*, 2000, vol. 3, pp. 394–396.
19 Y. Li, J. A. Nemes and A. A. Derdouri, *Polym. Eng. Sci.*, 2001, **41**, 1399–1412.
20 E. Verron, G. Marckmann and B. Peseux, *Int. J. Numer. Meth. Eng.*, 2001, **50**, 1233–1251.
21 E. Verron and G. Marckmann, *Int. J. Non Linear Mech.*, 2003, **38**, 1221–1235.
22 F. Tanaka and S. F. Edwards, *Macromolecules*, 1992, **25**(5), 1516–1523.
23 F. J. Vernerey, *J. Mech. Phys. Sol.*, 2018, **115**, 230–247.
24 J. G. Williams, *Int. J. Fract.*, 1997, **87**, 265–288.
25 B. Nadler and T. Tang, *Int. J. Non Linear Mech.*, 2008, **43**, 716–721.
26 R. Long, K. R. Shull and C. Y. Hui, *J. Mech. Phys. Sol.*, 2010, **58**, 1225–1242.
27 J. Shi, S. Müftü and K. T. Wan, *J. Adhes.*, 2011, **87**, 579–594.
28 A. Srivastava and C. Y. Hui, *Proc. R. Soc. A*, 2013, **469**, 20130424.
29 N. Kumar and A. Dasgupta, *Int. J. Non Linear Mech.*, 2013, **57**, 130–139.
30 V. A. Eremeyev and K. Naumenko, *Mech. Res. Commun.*, 2015, **69**, 24–26.
31 G. Li and K. T. Wan, *J. Adhes.*, 2010, **86**, 969–981.
32 C. Y. Hui and R. Long, *J. Adhes.*, 2012, **88**, 70–85.
33 R. Long and C. Y. Hui, *Int. J. Solids Struct.*, 2012, **49**, 672–683.
34 A. Srivastava and C. Y. Hui, *Proc. R. Soc. A*, 2014, **470**, 20140528.
35 H. Chen, X. Feng, Y. Huang, Y. Huang and J. A. Rogers, *J. Mech. Phys. Solids*, 2013, **61**, 1737–1752.
36 R. Mangan and M. Destrade, *Int. J. Non Linear Mech.*, 2015, **68**, 52–58.
37 J. Y. Faou, G. Parry, S. Grachev and E. Barthel, *Phys. Rev. Lett.*, 2012, **108**, 116102.
38 J. Simo and D. Fox, *Comput. Methods Appl. Mech. Eng.*, 1989, **72**, 267–304.
39 F. J. Vernerey, R. Long and R. Brighenti, *J. Mech. Phys. Solids*, 2017, **107**, 1–20.
40 S. L. Sridhar and F. J. Vernerey, *Polymers*, 2018, **10**(8), 848.
41 T. Shen, R. Long and F. Vernerey, *Comput. Mech.*, 2019, **63**, 725–745.
42 G. Holzapfel, *Nonlinear solid mechanics: a continuum approach for engineering*, 2000, 1st edn, p. 455.
43 A. Wineman, *Comput. Math. Appl.*, 2007, **53**, 168–181.
44 E. Benet, H. Zhu and F. J. Vernerey, *Phys. Rev. E*, 2019, **042502**, 1–12.
45 A. L. Flory, D. A. Brass and K. R. Shull, *J. Polym. Sci., Part B: Polym. Phys.*, 2007, **45**, 1390–1398.
46 M. Barquins and M. Ciccotti, *Int. J. Adhes. Adhes.*, 1997, **17**, 65–68.

47 M. Hossain, D. K. Vu and P. Steinmann, *Comput. Mater. Sci.*, 2012, **59**, 65–74.
48 T. H. Lengyel, Y. Qi, P. Schiavone and R. Long, *J. Mech. Phys. Solids*, 2016, **90**, 142–159.
49 T. Shen, J. Kan, E. Benet and F. J. Vernerey, *Soft Matter*, 2019, DOI: 10.1039/C9SM00911F.
50 C. Keplinger, T. Li, R. Baumgartner, Z. Suo and S. Bauer, *Soft Matter*, 2012, **8**, 285–288.
51 S. Song and M. Sitti, *Adv. Mater.*, 2014, **26**, 4901–4906.
52 Z. Ye, G. Z. Lum, S. Song, S. Rich and M. Sitti, *Adv. Mater.*, 2016, 5087.
53 F. J. Vernerey, R. Brighenti, R. Long and T. Shen, *Macromolecules*, 2018, **51**, 6609–6622.